ORIGINAL ARTICLE

Mechanical investigation of glass ceramic brazed ceramic and steel composites

Tobias M. Walter [iD]　|　Ethel C. Bucharsky [iD]　|　Karl G. Schell　|　Michael J. Hoffmann

Institute of Applied Materials – Ceramic Materials and Technologies (IAM-KWT), Karlsruhe Institute of Technology, Karlsruhe, Germany

Correspondence
Tobias M. Walter, Institute of Applied Materials – Ceramic Materials and Technologies (IAM-KWT), Karlsruhe Institute of Technology, Karlsruhe 76131, Germany.
Email: tobias.walter@kit.edu

Funding information
Bundesministerium für Wirtschaft und Energie, Grant/Award Number: 03ET6112C

Abstract

Solid oxide fuel cells (SOFC) convert chemical energy from hydrogen, methane, or other hydrocarbons directly into electrical energy and heat. Advantages are low noise during operation as well as relatively low pollutant emissions. This makes them interesting for stationary applications, eg combined heat and power plants for domestic use and for mobile applications, when there is a demand for integrating auxiliary power units. The high operating temperatures of about 850°C and the simultaneous presence by both, reducing and oxidizing atmospheres place high demands on the components of a SOFC. Due to these requirements, glass-ceramics are proposed as sealants between interconnector and electrolyte. They provide lower costs and lower weight than commercially used silver solders. Furthermore, they have the following impressive benefits: The sealants are electrical insulating, chemical stable and by careful materials selection and adapted manufacturing processes, they adhere well on steel and on ceramic substrates. In order to characterize the adhesion of glass-ceramic sealants on steel and on zirconia substrates, layer-like composites are fabricated by screen-printing and subsequent sintering in air. It turns out that the formation of crystalline phases at the interface is crucial for the adhesion behavior.

KEYWORDS

Charalambides, composites, Glass-ceramic-sealant, mechanical testing, SOFC

1 | INTRODUCTION

There are several ways to store secondary energy. These types of energy sources often depend on the weather or climate to work effectively, and include such methods as wind power, solar power, gas technology, and hydroelectricity in its many forms.[1-4] Actually, a reuse of stored energy in fuels like methane or hydrogen is possible eg with a solid oxide fuel cell (SOFC). SOFCs are a type of power source conversion device that can transform hydrogen or hydrocarbon gases into electricity at temperatures of 700-1000°C.[5-6] SOFC cells consist principally of three layers: cathode/ electrolyte/ anode. It is

important that leaks are avoided and electrical insulation between the layers is ensured. For this reason, the sealant must provide hermeticity between the system components.

Commercially available SOFCs mostly use silver solders that have been examined in several studies, eg see Kuhn et al.[7-10] In order to reduce costs in the production of a SOFC the use of glass sealings is discussed because they are electronic insulating as well as thermally, chemically and mechanically stable. In addition to the realization of the joining of metallic interconnector sheets used in planar SOFC, a glass-ceramics sealing can also be used to join the ceramic electrolyte on ferritic steel.

In this work, glass solders for joining steel or ceramics are investigated. The focus is on the development of the soldering process that is evaluated on the basis of the time- and temperature-dependent microstructure formation and the achievable adhesion for the individual thermal treatments. The glass solder layer is based on a composition patented by Durschang[11] and is printed on the substrates by screen printing. The subsequent soldering process is done in air, but under an applied uniaxial load. The most important parameters are temperature and time, which are systematically investigated and their influence on the soldering process is evaluated and discussed. To account the different joining partners a ferritic steel- and zirconia as ceramic substrates are used.

For mechanical characterization, a modified four-point bending test according to Charalambides et al[12,13] was used to evaluate the adhesion considering different soldering conditions. In order to estimate crystal phases quantitatively, SEM and EDX images of cross-sections were used to determine the area fraction of the individual phases. As a result, these two quantities can be related to each other.

2 | EXPERIMENTAL PROCEDURE

2.1 | Materials and sample preparation

In order to compare adhesion between glass ceramic and the individual substrate materials, suitable samples must be prepared for each interface combination. The tested interfaces are glass-ceramic on steel (Crofer 22 H®) and glass-ceramic on two types of zirconia.

For zirconia, TZ-8Y and TZ-3Y (Fully stabilized zirconia with 8 mol % and tetragonal zirconia polycrystal with 3 mol % yttria, respectively; both TOSOH, Japan) powder is prepressed and afterwards isostatically pressed at 400 MPa into rectangular plates with the dimensions ($65 \times 45 \times 4$ mm^3) at 400 MPa. Thereafter, the plates were sintered at 1500°C (3Y-TZP) and 1600°C (8Y-CSZ) with a heating rate of 2 K/min, and held for 3 hours. After slow cooling (appr. 2K/min) the samples are taken out and ground either to substrates ($2.5 \times 7 \times 45$ mm^3) or to stiffening elements ($2.5 \times 7 \times 22$ mm^3) needed for the bending tests, see Figure 1.

The screen-printing paste is based on a fritted alumina-borosilicate glass (basic composition: appr. 20 mol% MgO, 10 mol% CaO, 10 mol% B_2O_3, 5 mol% Al_2O_3, 45 mol% SiO_2 and in sum 8 mol% ZrO_2 and Y_2O_3, for details see 11,14). The frit was milled in a planetary ball mill to powder until a particle size of d_{50} = 5-30 μm was achieved.[14] Subsequently, the glass powder was dispersed in an organic suspension medium and screen printed as described in Dittrich et al.[15] Glass layers of about 100 μm thickness were screen-printed with a printing paste having 50 volume % solid-content. The two 20 mm × 5 mm glass layer traces were screen printed on substrate material by SD 05 (Roku Print) as shown in Figure 1.

2.2 | Soldering process

The stiffening elements were placed on the previously screen-printed layers and the composites were heated at 5 K/min to 450°C under a load of 120 kPa and kept for 30 min to burn out the organic. In a second step, the samples are further heated to the final temperature. For the adhesion test of the glass-ceramic sealant/steel composite, the sintering temperature is varied from 860°C to 930°C and samples are either cooled immediately after reaching the temperature or held there for two hours. Cooling to room temperature was carried out at a cooling rate of up to 5 K per minute.

2.3 | Mechanical characterization

The mechanical characterization is based on a four-point bending test according to Charalambides[13], modified by Hofinger et al[12], which allows the calculation of the energy release rate (G_{SS}) when driving a crack between substrate and solder:

$$G_{SS} = \frac{M_b \cdot \left(1 - v_{\text{sub.}}^2\right)}{2 \cdot E_{\text{sub.}}} \cdot \left(\frac{1}{I_y} - \frac{1}{I_c}\right) \quad (1)$$

Equation (1) contains Young's Modulus E and Poisson's ratio v of the substrate material as well as the sealant
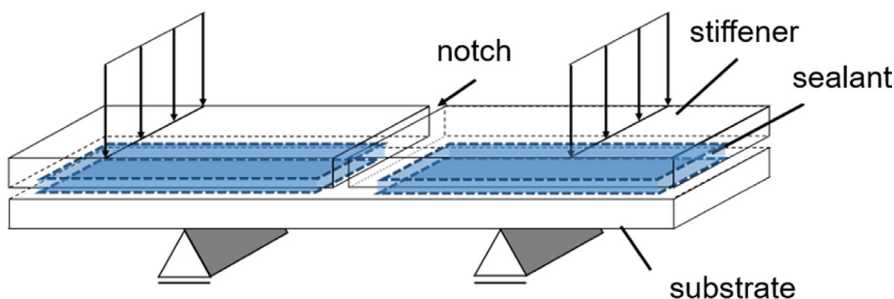

FIGURE 1 Components of a built-in sample of the modified four-point bending test after Charalambides[13]. Representation according to Hofinger et al[12] [Color figure can be viewed at wileyonlinelibrary.com]

material (see (5)) and the applied moment M_b, that is calculated by:

$$M_b = \frac{P \cdot l}{2 \cdot b} \tag{2}$$

where P is the applied load, l the distance between inner and outer supports ($l = 10$ mm) and b the width of the substrate.

Further, in Equation (1) there is the second moment of inertia, I_y, that is described as:

$$I_y = \frac{h_{\text{sub.}}^3}{12} \tag{3}$$

with h_{sub} as the thickness of the bar-shaped substrate. Using the parallel-axis-theorem results in a correction of the second moment of inertia which is abbreviated by I_c. Assuming as a simplification that the substrate and stiffener material are the same ($\mu = 1$) and of the same thicknesses (see Hofinger et al[12]), the correction of the moment of inertia is expressed by:

$$I_c = \frac{2}{3} h_{\text{sub}}^3 + \frac{1}{12} \kappa \cdot h_l^3 + h_{\text{sub}}^2 \cdot h_l + \frac{1}{2} \cdot h_{\text{sub}} \cdot h_l^2 \tag{4}$$

with the thickness of sealant layer h_l, and an expression named κ, that is defined as:

$$\kappa = \frac{E_l \cdot \left(1 - v_{\text{sub}}^2\right)}{E_{\text{sub}} \left(1 - v_l^2\right)} \tag{5}$$

For calculating the energy release rate, all Poisson ratios were assumed to be 0.3. The Young's Modulus was determined using the resonance method (MK5i, GrindoSonic, Belgium) according to DIN 843-2.[16] The Young's moduli are $E_l = 104$ GPa for the glass ceramic layer, $E_{\text{sub.TZP}} = 210$ GPa and $E_{\text{sub.CSZ}} = 174$ GPa for ceramic and $E_{\text{sub.steel}} = 208$ GPa for steel (this value is taken from the data sheet[17]). A change in modulus of elasticity E_l and the Poisson number due to the transformation from glass to glass ceramic was neglected.

2.4 | Microscopic investigation

SEM-images were collected in order to characterize the microstructure, whereas energydispersive X-ray spectroscopy (EDS) was performed for the elemental analysis in order to gain insights on the developed phases. As important parameters, the area fractions of the crystal phases in comparison to the residual glass and the pore fraction were determined from the micrographs of the cross-sections. For this, samples were cut with a wire saw, embedded in epoxy resin and polished stepwise with using diamond suspensions up to 0.25 μm.

3 | RESULTS AND DISCUSSION

3.1 | Densification and crystallization

To obtain information on the densification behavior, porosity evolution was studied over time and temperature. The results are shown in Figure 2. The porosity remains approximately constant for temperatures below 720°C indicating that densification starts above 720°C. After this temperature the relative porosity decreases and consequently the thickness of the printed glass layer begins to shrink. At 860°C it can be assumed that densification is completed, since the porosity is close to zero. Looking at the microstructure shown in Figure 3A), one can see that no particle boundaries exist anymore. For the thermally treated samples with the same temperature condition, but with a hold time of 2 hours, (filled white squares in Figure 2), the porosity values are lower indicating that with a longer hold time the sintering process at 800°C is completed.

The SEM images of the microstructure, Figure 3, show that a crystallization process occurs when the samples were treated in the temperature range between 860°C and 930°C and hold times up to two hours. The different phases which can be seen in the images of Figure 3 are quartz, enstatite, and zirconium rich crystalline phases (including baddeleyite and zircon) as well as pores and residual glassy phase. In the temperature range from 860°C to 930°C the crystallization of the homogeneous glassy layer to a glass ceramic occurs. This can be seen in more detail in Figure 4A,B, where the areas of the images were allocated proportionally to the phases and the relative proportion of each phase was averaged with four image values.

In general, areas of 2000 to 5000 square micrometres were evaluated. A mean error of 2% was found when comparing the images of a parameter variation.

As can be concluded from a comparison of Figure 4A,B, the hold time has an important influence on the crystallization process. For samples heat treated between 860 and 930°C without hold time, no significant crystal formation, with the exception of quartz, up to 3% of the total phase, was observed. However, this changes when applying longer hold times: the proportion of enstatite- and zirconium-containing crystals increase as the temperature increases (Figure 4B). In particular, the proportion of the enstatite crystals grow up to 24% at 900°C and over 30% of the total composition at 930°C. The enstatites first crystallize at the interface, so a heterogeneous nucleation can be assumed. The crystal formation at the interface should have a greater influence on the adhesion properties than a crystallization in volume.
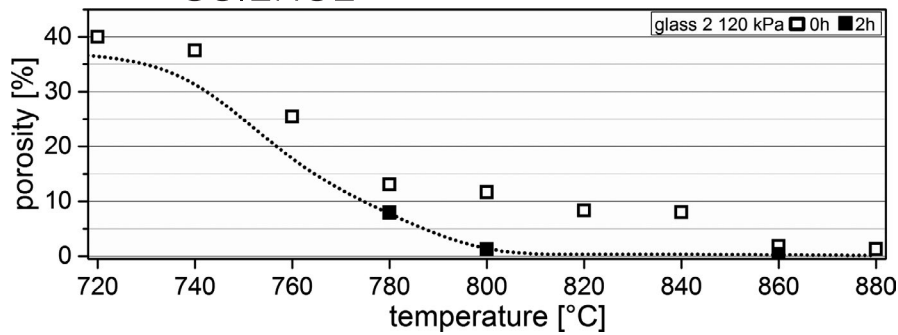
FIGURE 2 Dependence of the average relative porosity on the temperature (680°C to 930°C) of the controlled termination of the test (black squares), the minima values of the relative porosity measurements of the termination experiments (dashed plot) and average relative porosity with a 2-h hold time (white filled squares)

3.2 | Mechanical testing of the composite: Glass-ceramic-sealant/steel

To carry out mechanical tests, a homogeneous glass layer is needed, which has to adhere to both joining partners. In addition, the glass particles must form a continuous layer, so that sufficient strength is achieved. From about 860°C the densification appears to be complete, which is shown by a homogeneous glass phase, see Figure 3A.

The determined energy release rates (G_{SS}), which are a measure of the quality of adhesion of the joined materials, are shown in Figure 5 normalized to an equal joining width of 7 mm. Regarding the soldering process, it should be noted that there is a mismatch in thermal expansion of the individual materials. For the glass solder a CTE of 8.1×10^{-6} K^{-1} and for the ceramic a value of 10.2×10^{-6} K^{-1} between room temperature and 500°C is given in 14 while the used steel substrate has a higher value of 11.0×10^{-6} K^{-1}[17]. Accordingly, the glass solder has the smallest coefficient of thermal expansion, which means that stresses are built up from the point at which the temperature during cooling falls below T_g. This leads to compressive stresses in the glass, while the substrate is stressed in tension. However, since the substrate is comparatively thick, the latter can be neglected. Nevertheless, stresses remain, which probably have an influence on the energy release rate. However, since all the variants examined have the same conditions, the results are at least comparable with each other.

The adhesion of the still amorphous glass layer shows a lower energy release rate than a crystallized glass-ceramic layer, see Figure 5. As the temperature increases, the values for G_{SS} of the glass-ceramic-sealant/steel composite increase for two hours holding time. At the highest investigated temperature of 930°C, the differences between the two series of tests become minimal, which is why it can be assumed that soldering is already complete. It turns out, however, that the hold time is quite helpful, since higher energy release rates are achieved even at lower temperatures. So, there is a shift to lower temperatures and from 900°C on, a maximum in energy release rate is reached. Considering the microstructure and the developed phases, the formation of enstatite crystals in the interface region seems to be responsible for the better adhesion. Accordingly, comparable interface areas can be seen in Figure 3B,E even that the sintering

parameters, 880°C (hold time of two hours) and 930°C (without hold time), being quite different. Both figures show similar crystal phase distributions at the interface despite the sintering parameters, so that the energy release rates are almost identical (see Figure 5). The samples that were treated at a lower temperature do not show any crystallized areas in the SEM image, which is why they are not shown here. The energy release rate thus seems to be dependent on the fraction of interface covered with enstatite. A maximum of G_{SS} can be achieved using a sintering temperature of 900°C and a hold time of two hours. To reach the maximum of adhesion, it does not seem to make any difference whether the enstatite crystals need to be particularly large or have a certain relative proportion, but a continuous enstatite layer of 3 to 4 micronmeter at the interface seems to be beneficial.

3.3 | Mechanical testing of the composite glass-ceramic-sealant/ceramic

In addition to investigations of the layer adhesion of the glass ceramic to the joining partner steel, ceramics were also investigated as substrate material. Experiments with the joining partner steel indicate that the maximum adhesion occurred after soldering at 900°C for two hours. Therefore, this parameter set was used for the tests with ceramic as a substrate. Because the glass-ceramic sealant adheres well to the 8Y-CSZ ceramic substrate, the substrate breaks rather than cracking along the interface. This is partly due to the strong adhesion, on the other hand, it is due to the relatively low fracture toughness of the 8-CSZ. As a result, the CSZ ceramic breaks, the composite remains (see Figure 6). For this reason, an energy release rate can only be estimated according to the work of He and Hutchinson.[18] Therefore, it requires a substrate material with higher fracture toughness, so instead of 8-CSZ tetragonal zirconia polycrystals (3Y-TZP) is used (see Figure 8).

By changing the substrate material, the crack could be held at the interface (see Figure 3F), which is why the Charalambides test provides evaluable results. This test revealed energy release rates $G_{SS,TZP}$ of about 15N/m for 900°C sintering temperature and a holding time of two hours (see Figure 5) that is close to G_{SS}-values for composites with steel substrates. Considering the microstructure of the glass-ceramic-sealant in combination with

FIGURE 3 Exemplary SEM images from cross-sections of the sealed glass ceramic compound with steel- (A-E) and a PSZ-ceramic (F). Samples are sintered with a load of 120 kPa and sintering temperature from 860°C to 930°C and 2-h hold time (A-D and F) and once in a termination experiment with no hold time at maximum temperature (E). In the pictures some phases are marked with the abbreviations: Including quartz phase (dark spots, Q) zirconium containing phases (white spots, Z), pores (black areas, P), enstatite phases (highlighted grey areas, E), and residual glass phase (grey background)
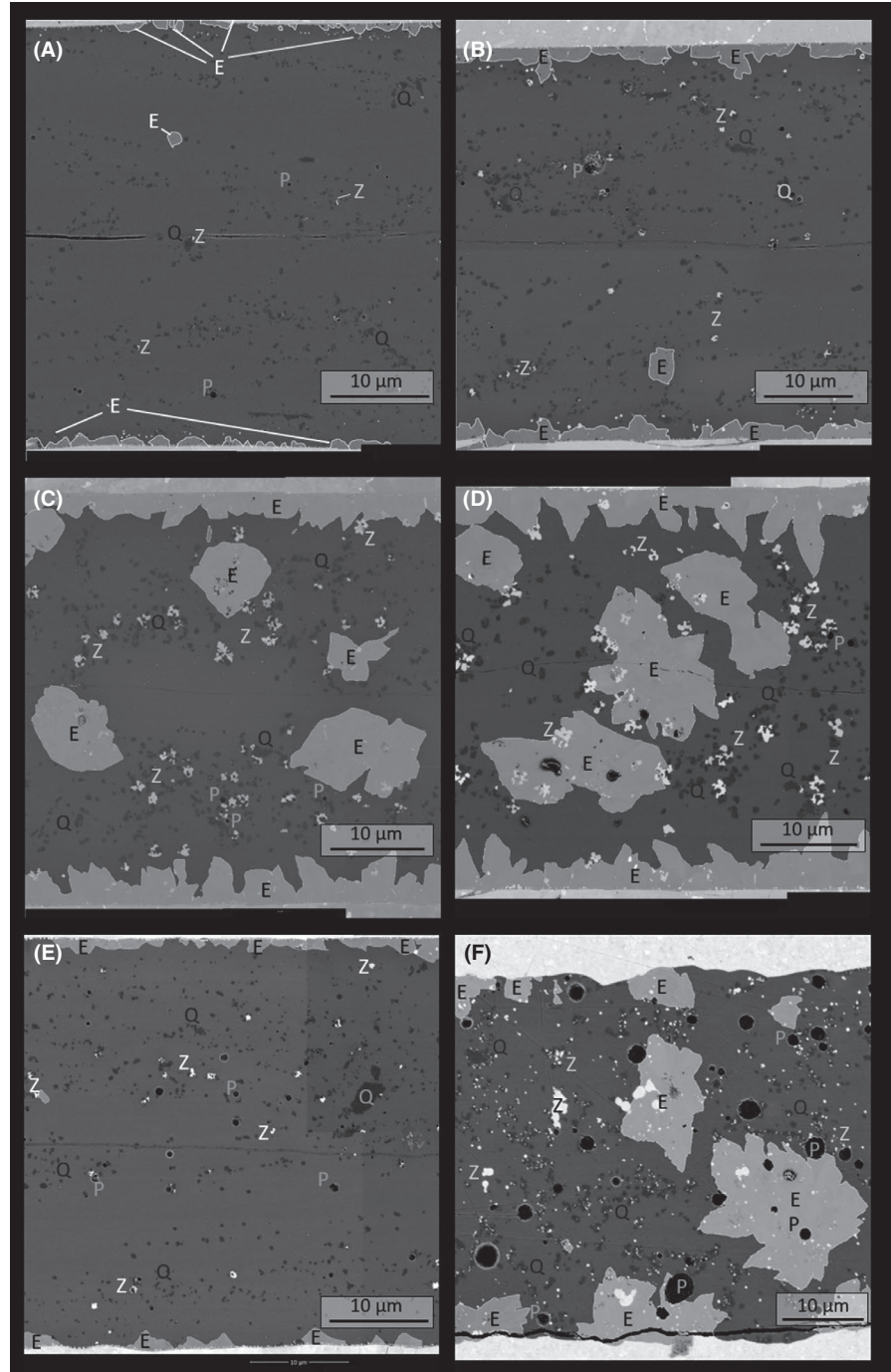
the 3Y-TZP ceramic, the same crystalline phases are visible as in the steel composites. Also the enstatite crystals are formed at the interface that according to our working hypothesis probably hinders crack propagation and leads to a higher energy release rate. From this we conclude that the formation of these near-interface enstatite crystals is responsible for the increased adhesion of the glass sealant to both individual joining partners. As already mentioned, the G_{SS_CSZ} can be estimated by the model of He and Hutchinson.[18] Two cases are distinguished where the crack either runs along the interface (eg 3Y-TZP, see Figure 3F)) or passes through the substrate material (eg CSZ, see Figure 6). Thus, if the crack propagates along the interface, the adhesion

can be quantified with the energy release rate G_{SS} according to (1). In the second case, energy is released by forming new surfaces which can be described best by the strain energy release rate G_{sub} of the substrate material, which follows

$$G_{sub.} = \frac{K_{IC}^2}{\overline{E}_{sub}} \tag{6}$$

where $\overline{E}_{sub}$ and $\overline{E}_l$ are defined as:

$$\overline{E}_{sub} = \frac{E_{sub}}{\left(1 - v_{sub}^2\right)}; \quad \overline{E}_l = \frac{E_l}{\left(1 - v_l^2\right)} \tag{7}$$
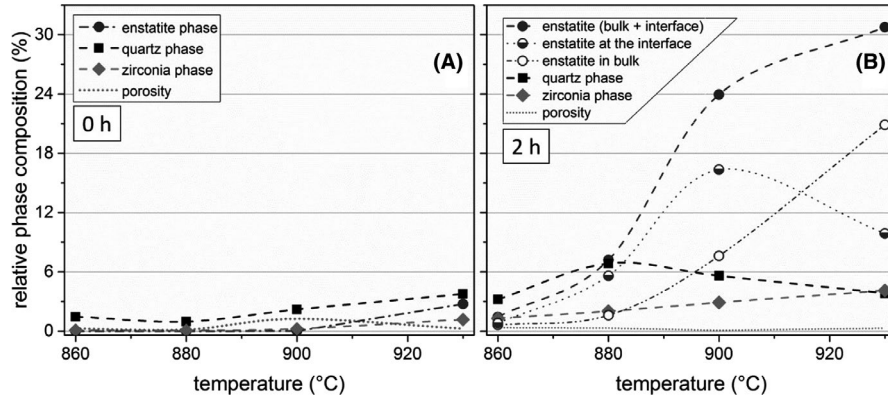
FIGURE 4 Relative phase composition in the sintered glass ceramic for a glass ceramic/steel compound for (A) termination experiments and (B) a 2-h hold time. Shown are quartz phase (black square), zirconium containing phase (gray diamond), porosity (gray dotted plot), and enstatite phase (circle), (B) that is divided into enstatite form the interface with steel (half-filled circle) and enstatite been present only in the glass ceramic (white filled circle)

With the consideration of He and Hutchinson, it can be clarified under which circumstances which of the two cases applies. Thus, in their model, they analytically approximated the conditions of the two cases with a function that depends inter alia on the ratio of the different energy release rates G_{SS} to G_{sub} and a parameter α, which can be calculated by

$$\alpha = \frac{\overline{E}_{sub} - \overline{E}_l}{\overline{E}_{sub} + \overline{E}_l} \tag{8}$$

By combining Equations (7) and (8) it yields for α:

$$\alpha = \frac{E_{sub}\left(1 - v_l^2\right) - E_l\left(1 - v_{sub}^2\right)}{E_{sub}\left(1 - v_l^2\right) + E_l\left(1 - v_{sub}^2\right)} \tag{9}$$

As shown by He and Hutchinson,[18] the ratio of the two energy release rates (G_{SS}/G_{sub}) vs α has to be considered. For example, using the measured Young's moduli and setting the Poisson's ratios to $v = 0.3$, as described in Section 2.3, α results in a value of 0.23. From this, an energy release rate ratio for both edge conditions can be determined. By projecting the intersection of the function at α equal to 0.23 with the abscissa (see figure 11 in 18), the energy release rate $G_{SS,CSZ}$ is approximately 30% of the substrate G_{sub}. As seen in Figure 7, energy release rates of maximum 30 N/m can occur for CSZ ceramics. Taking that into account and the determined ratio of G_{SS} to G_{sub}, a value greater than 9 N/m can be expected for $G_{SS,CSZ}$.

Considering the microstructure of the glass sealant at the interfaces to the CSZ- and TZP- ceramics, a similar picture emerges (see Figures 3F and 8). So the microstructure appears almost identical. Assuming that the energy release rate G_{SS} is proportional to the amount of enstatite crystals at the substrate interface, it is possible to go further and set the $G_{SS,}$
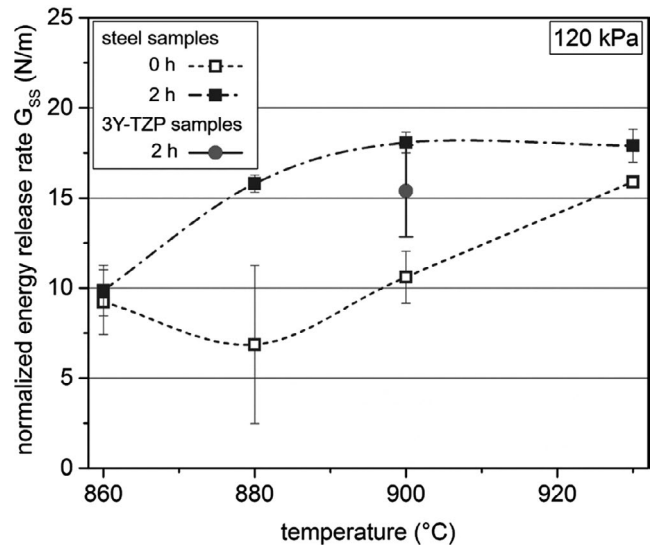

FIGURE 5 Energy release rates (normalized to a joining width of 7 mm) plotted against temperature (860°C to 930°C) for a glassceramic/metal interface for 2-h hold time (black squares), zero hours (white filled Squares) and for glass ceramic/TZP interface at 900°C and 2-h hold time (grey circle)

CSZ to be similar to $G_{SS, TZP}$. So $G_{SS, CSZ}$ can be assumed with a value close to 15 N/m for 900°C sintering temperature and 2-hour hold time.

4 | CONCLUSION

For the used glass sealant, an alumina-borosilicate glass, an optimum adhesion on steel at 900°C to 930°C and 2 hours hold time was achieved. According to our working hypothesis, the increase in adhesion can be directly correlated with the formation of enstatite crystals at the interface, which inhibits crack propagation along the interface. This result is based on a test according to Charalambides that provides

FIGURE 6 Stitched SEM image after mechanical testing showing a broken ceramic substrate (8Y CSZ)
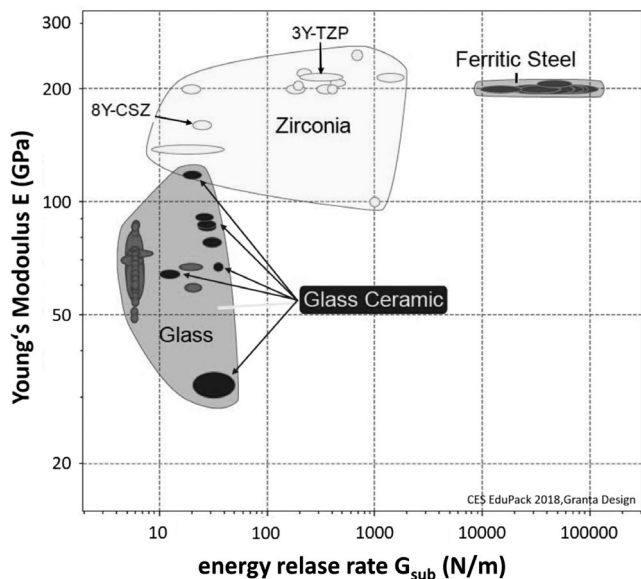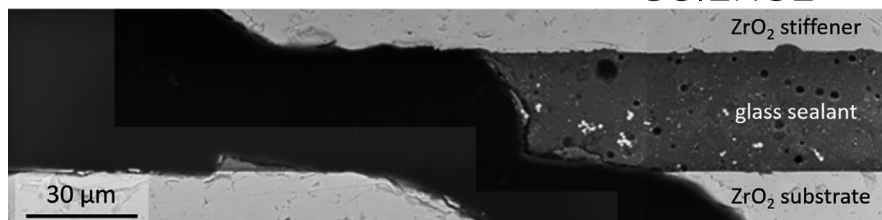

FIGURE 7 Ashby diagram for glass, glass ceramics, zirconia and ferritic steel based on data from CES EduPack, Granta Design

valuable insights into the adhesion behavior, whereby the process conditions of soldering can be evaluated. Hence a process window can be quantitatively determined.
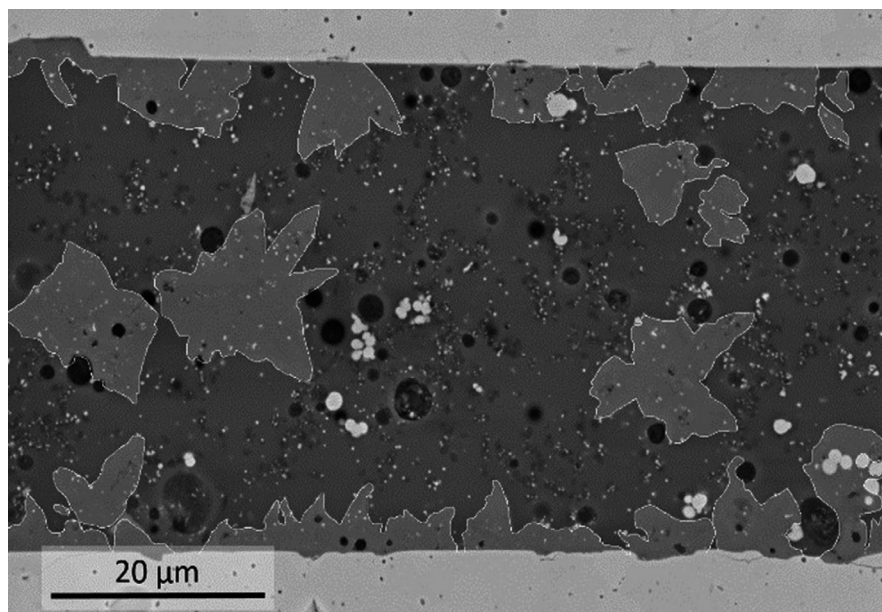
In addition, the glass sealant was used to join in conjunction with zirconia (3Y-TZP and 8Y-CSZ). The optimum sintering parameters of the ferritic steel (900°C and 2 hours) were transferred to these material joints. Comparing Figures 3F and 8 (ceramics) with Figure 3C

) (ferritic steel) shows, despite different joining partners, similar microstructures form. It turns out that higher energy release rates are accompanied by a higher enstatite content, as shown in the corresponding SEM images. This tendency holds for all microstructures of the glass ceramic joints. Also the mechanical Charalambides test shows similar results for 3Y-TZP. There, the G_{SS} is slightly below the energy release rate of steel, which correlate with the slightly lower enstatite content at the ceramic interface.

The cubic stabilized zirconia normally used as electrolyte could not be mechanically tested, because of its brittle behavior. Nevertheless, a similar energy release rate can be assumed because of the identical microstructure of both ceramic seals. The results of He and Hutchinson[18] provided a theoretical approximation of the G_{SS} at which the cubic stabilized Zirconia components can be mechanically tested. This is one-half to one-third of the theoretical value of the strain energy release rate of zirconia, which is why the CSZ ceramic substrate breaks instead of the sealing. As a consequence of these results, it can be assumed that the sealed glass-ceramic sealant is mechanically much more stable than the electrolyte. This, as well as the lower costs of raw materials and processing makes the used alumin-aborosilicate glass sealant a true, cost effective, and excellent alternative to silver solder joining.

FIGURE 8 SEM images from cross-sections of the sealed glass ceramic compound with 8Y-CSZ-ceramic sintered with a load of 120 kPa and sintering temperature from 900°C and 2-h hold time with enstatite phases (highlighted grey areas)

ORCID

Tobias M. Walter 🄳 https://orcid.org/0000-0002-2044-5416
Ethel C. Bucharsky 🄳 https://orcid.org/0000-0001-8236-119X

REFERENCES

1. Agora Energiewende – Jahresauswertung 2017 (engl.: annual report 2017) [updated 2017 Dec; cited: 2019 Dec 6]. Available at https://www.agora-energiewende.de/projekte/jahresauswertung-2017/
2. Agora Energiewende-Der Stromsektor der EU 2017(engl.: The electricity sector in the EU-2017) [updated 2018 Jan; cited: 2019 Dec 6]. Available at https://www.agora-energiewende.de/projekte/der-stromsektor-der-eu-2017/
3. Agorameter - Dokumentation-Version 9.1 - Stand Oktober 2019 (engl.: documentation-version 9.1-status october 2019) [updated 2019 Oct; cited:2019 Dec 6]. Available at https://www.agora-energiewende.de/veroeffentlichungen/agorameterdokumentation/
4. Götz M, Lefebvre J, Mörs F, McDaniel Koch A, Graf F, Bajohr S, et al. Renewable power-to gas: a technologic and economic review. Renew Energy. 2016;85:1371–90.
5. Kaur G. Solid Oxide Fuel Cell Components: Interfacial Compatibility of SOFC Glass Seals. Cham: Springer, 2016.
6. Basu RN. Materials for Solid Oxide Fuel Cells. In: Basu S, editor. Recent trends in fuel cell science and technology. New Dehli, India: Anamaya Publisher, Springer, 2007; p. 286–331.
7. Brandenberg J, Kuhn B, Pausch M, Beck T, Singheiser L. Testing of mechanical performance of reactive-air-brazed (RAB) metal/ceramic joints for SOFC-applications. EFCF. 2011;B1003:1–14.
8. Kuhn B. Bruchmechanische Untersuchungen von Metall/Keramik-Verbundsystemen für die Anwendung in der Hochtemperaturbrennstoffzelle (engl: Fracture Mechanical Investigations of Metal/Ceramic Composite Systems for Application in High Temperature Fuel Cells). Energy Environ. 2012;50:1–118.
9. Skiera E, Brandenberg J, Li C, Beck T, Singheiser L, Kuhn B. Mechanical properties of reactive air brazed (RAB) Metal/Ceramic Joints. Part 1: Visco-plastic deformation of silver-based reactive air brazes. Adv Eng Mater. 2014;16(12):1462–7.
10. Skiera E, Brandenberg J, Li C, Koppitz T, Beck T, Singheiser L, et al. Mechanical properties of reactive air brazed (RAB) metal/ceramic joints. Part 2: tailored microstructure for thermal cycling resistance. Adv Eng Mater. 2014;16(12):1423–9.
11. Durschang B.Use of an alkali-free silicon, magnesium and heavy alkaline earth metal oxide mixture as a high thermal expansion coefficient glass-ceramic joint material, especially for high temperature fuel cells. German patent 198 57 057 C1, 2000.
12. Hofinger I, Oechsner M, Bahr HA, Swain MV. Modified four-point bending specimen for determining the interface fracture energy for thin brittle layers. Int J Fract. 1998;92:212–20.
13. Charalambides PG, Lund J, Evans AG, McMeeking RM. A test specimen for determining the fracture resistance of bimaterialinterfaces. J Appl Mech. 1989;56:77–82.
14. Hauber S, Dittrich S, Walter TM, Durschang B, Schell KG, Bucharsky EC, et al. Bilayered glass-ceramics as sealants for SOFC. J Mat Sci Eng. 2019;A9(3–4):43–55.
15. Dittrich S, Reitz E, Schell KG, Bucharsky EC, Hoffmann MJ. Development and characterization of inks for screen printing of glass solders for SOFCs. ACT. 2020;1–10.
16. DIN EN. 843–2:2006–12. Advanced technical ceramics – Mechanical properties of monolithic ceramics at room temperature - Part 2: Determination of Young's modulus, shear modulus and Poisson's ratio.
17. Krupp T.Crofer® 22 H material data sheet No. 4050; June 2010.
18. He MY, Hutchinson JW. Crack Deflection at an interface between dissimilar Elastic Materials. Int J Solids Structures. 1989;25(9):1053–67.

How to cite this article: Walter TM, Bucharsky EC, Schell KG, Hoffmann MJ. Mechanical investigation of glass ceramic brazed ceramic and steel composites. *Int J Appl Glass Sci*. 2021;12:175–182. https://doi.org/10.1111/ijag.15822